ACS APPLIED MATERIALS & INTERFACES

Research Article

www.acsami.org

Dielectric Properties of Polymer–Particle Nanocomposites Influenced by Electronic Nature of Filler Surfaces

Sasidhar Siddabattuni,[†] Thomas P. Schuman,*[,†] and Fatih Dogan[‡]

[†]Chemistry Department, Missouri University of Science and Technology, 400 W. 11th Street, Rolla, Missouri 65409, United States

[‡]Materials Science and Engineering Department, Missouri University of Science and Technology, 1400 N. Bishop Avenue, Rolla, Missouri 65409, United States

Supporting Information

ABSTRACT: The interface between the polymer and the particle has a critical role in altering the properties of a composite dielectric. Polymer-ceramic nanocomposites are promising dielectric materials for many electronic and power devices, combining the high dielectric constant of ceramic particles with the high dielectric breakdown strength of a polymer. Self-assembled monolayers of electron rich or electron poor organophosphate coupling groups were applied to affect the filler–polymer interface and investigate the role of this interface on composite behavior. The interface has potential to influence dielectric properties, in particular the leakage and breakdown resistance. The composite films synthesized from the modified filler particles dispersed into an epoxy polymer matrix were analyzed by dielectric spectroscopy, breakdown strength, and leakage current measurements. The data indicate that significant reduction in leakage currents and dielectric losses and improvement in dielectric breakdown strengths resulted when electropositive phenyl, electron-withdrawing functional groups were located at the polymer–particle interface. At a 30 vol % particle concentration, dielectric composite films yielded a maximum energy density of ∼8 J·cm^{-3} for TiO_2-epoxy nanocomposites and ∼9.5 J·cm^{-3} for $BaTiO_3$-epoxy nanocomposites.

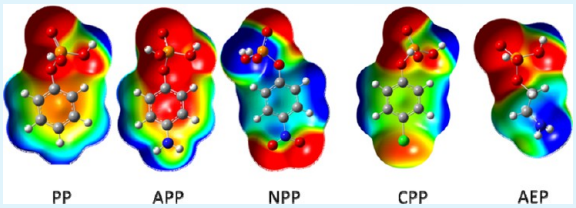

KEYWORDS: *interface, organophosphate, dielectric breakdown, permittivity, energy density*

INTRODUCTION

Nanodielectrics to store electrical energy play a key role in modern electronics and electric power systems. Conventional micrometer-sized particles are substituted with nanosized metal oxide particles in nanodielectric systems.[1−4] From eq 1, electrical energy storage density (U) in a linear dielectric material is proportional to the dielectric constant or permittivity of the material (k) and the square of the dielectric breakdown strength (DBS) (E_b).

$$U = kE_b^2/2 \quad (1)$$

An increased permittivity and/or DBS are required for greater energy storage density. While an increase in the composite dielectric constant can be obtained by increasing the volume fraction of high permittivity fillers, such as metal oxides, an improvement in DBS can play a more significant role in enhanced energy storage density.[5−7] Significant improvement in dielectric strength and other dielectric properties in nanocomposite systems is of interest to replace existing energy storage and insulation systems.[4,8,9]

Larger interfacial volume[10] exists in nanocomposites compared to microcomposites, and the properties of the interfaces between the polymer and the particles, which are nanometric in dimensions, are emphasized to be responsible for improvement in properties in nanodielectrics. Interfaces at the nanometric level are thought to exercise both passive and active control over dielectric properties of the composites[8,10] though we observe that the bare nanoparticle surfaces are inherently quite conductive. Improvement in the dielectric properties of nanodielectrics[8−11] could be due to several factors such as change in polymer morphology at the interface and local charge distributions because of nanoparticle surface; change in density and the energy depth of trap sites due to change in local structure at the interface, which affects the charge mobility and trapped state stability; increase in probability for scattering mechanism, and so forth. Thus, there is a potential to fabricate improved dielectric materials by manipulating the interface between filler and matrix without losing the dielectric characteristics of the bulk material.[12]

The advantages offered by large interfacial regions in nanodielectrics mainly depend on meeting new challenges in obtaining homogeneous dispersion of nanoparticles while avoiding particle agglomeration.[8,13] The addition of high surface energy ceramic particles into a low surface energy polymer creates highly inhomogeneous electric fields at the interfaces that can conduct charge due to improper and inhomogeneous dispersion, resulting in reduced DBS of the composites.[13,14] The addition of surfactants or surface coupling agents like organophosphates can balance surface tension to

Received: February 7, 2012
Accepted: March 1, 2013
Published: March 1, 2013

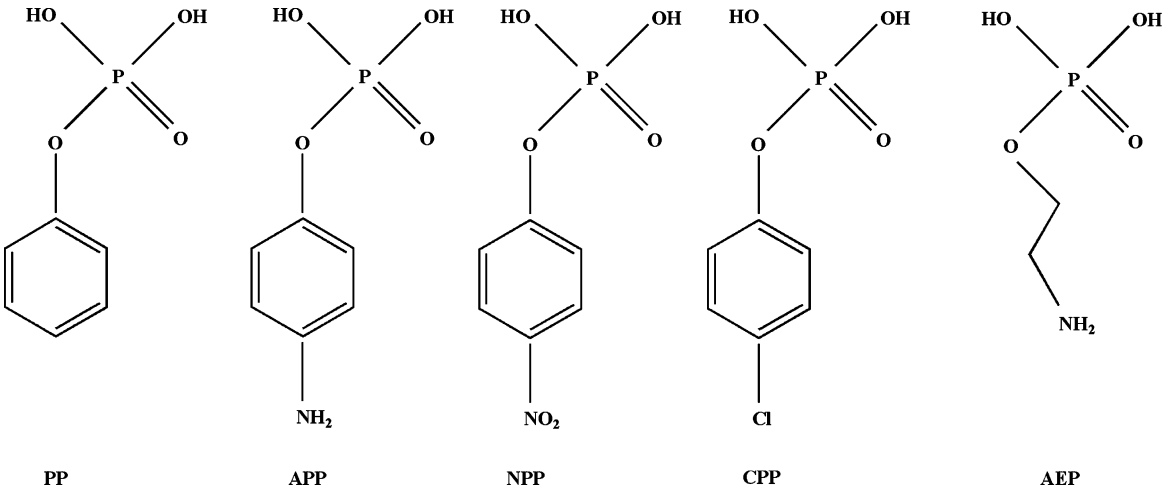

Figure 1. Molecular structures of SAM organophosphate ligands: phenyl phosphate (PP), aminophenyl phosphate (APP), nitrophenyl phosphate (NPP), chlorophenyl phosphate (CPP), and aminoethyl phosphate (AEP) used to modify the surface of TiO_2 before dispersing in polymer. For unmodified TiO_2, BYK-w-9010 was used as adsorbent surfactant while dispersing in polymer for comparison purpose.

improve dispersion and film quality compared to ceramic-particle composites without dispersing aids.[13−15]

Surface modification of nanoparticles through application of self-assembled monolayer (SAM) and relevance to dispersion quality, dielectric properties, and, in particular, DBS were studied previously.[14−20] Recent work has established that the particle surfaces and their composites are better controlled through chemical modification with organic ligands. Examples include organophosphonic acid modified, high dielectric constant particle dispersions in poly(vinylidene difluoride) (PVDF) that resulted in an estimated energy density of about 6.1 J·cm^{-3} at 50 vol % particles and a film thickness of about 3.84 μm thick.[16,20] The composite energy density was greater than the current state-of-the-art biaxially oriented polypropylene high energy density capacitors (1−3 J/cm^3).[15] However, little experimental work has studied the electronic nature of polymer−particle interface required to optimize the dielectric properties in polymer-ceramic nanocomposites. We further believe that establishing a correlation between interface control and dielectric properties is a major hurdle to the broader use and development of nanodielectrics technology.

We have sought to investigate how the structure of the interfacial layer between filler and polymer influences the dielectric properties of the composite. In the present work, we report dielectric nanocomposites of improved energy density that have resulted through electronic structure control placed at the filler interface. The control was achieved using SAM modification of metal-oxide nanoparticles with bifunctional organophosphate ligands, and the particles were then dispersed into relatively low loss epoxy polymer matrix composites. Electron donating or electron withdrawing functional groups, as part of the ligand structure, served to alter the polarity of the organophosphate ligand attached to the surface of filler particles. The surface functionalized fillers were used as inclusions in a polymer matrix and, based on their electronic nature, that is, electron donating or electron withdrawing, leakage current and dielectric loss and DBS of the composite film were affected.

A phosphate group may be attached to a benzene ring to synthesize a typical aromatic organophosphate ligand. Delocalized π electrons as an electron cloud exist in the benzene ring, a site of electron density that may be perturbed by the further addition of other functional groups to the phenyl ring. For example, Figure 1 shows the chemical structures of several organophosphate ligands that we examined as filler surface modifying ligands. Each ligand bearing a terminal functional group, electron donating (e.g., amine, NH_2) or electron withdrawing (e.g., nitro, NO_2; chloro, Cl), is perturbed in electronic structure because of polar and/or resonance effects compared to phenyl phosphate (PP). Phenyl phosphate, which does not bear any additional functional group on the phenyl ring besides the phosphate group, was considered as reference or "control" organophosphate group.[21]

The electron withdrawing or donating nature of attached functional groups has historically been used to influence the reactivity of the aromatic ring toward nucleophilic or electrophilic substitution reactions, that is, toward electron pair acceptance or donation by the phenyl ring, respectively. Therefore, the reactivity of the aromatic π electrons with an attached functional group is different from those of a benzene ring without functional group. Furthermore, an electric dipole will be induced by a functional group attached to a phenyl ring. Bound to the surface of filler particles, the groups influence control over the electronic structure at the filler−polymer interface.

The potential for a surface group to influence electron density and dielectric properties could be a useful from a synthetic perspective. In this context, we propose the hypothesis that a Hammett linear free energy relationship might be employed to correlate the electronic nature of interface with dielectric properties of polymer−particle nanocomposites to provide a tool for optimization of dielectric properties and energy storage density. A Hammett linear free energy relationship has been used to describe and rationalize the chemical structural differences of substituted phenyl groups toward chemical reactivity of aromatic organic compounds. Substituent functional groups that can be attached to aromatic benzene ring via para, meta, or ortho positions influences the free energy of ionization of the benzene ring because of different electronic effects of resonance and/or polarity, giving rise to differences in reaction rates.[22−24] The reactions in this case might be interactions of the modified filler surfaces with free electrons or ions migrating through the dielectric under the influence of the electric field. Established Hammett relation-

Table 1. TGA and XPS Measurement Data of Surface Modified and Unmodified TiO_2 and $BaTiO_3$ Nanoparticles

	TGA		XPS (atomic percent)					
powder	organic weight loss (%)	grafting density (groups/nm^2)	C (1s)	Ti (2p)	Ba (3d)	O (1s)	N (1s)	P (2p)
TiO_2	0.0		47.99	12.32		39.69	0.0	0.0
$BaTiO_3$ (BT)	0.0		28.48	13.18	8.50	46.35	3.50	0.0
NPP modi. TiO_2	1.3	1.4	19.73	21.45		56.22	0.71	1.90
APP modi. TiO_2	1.4	1.7	9.80	23.67		62.77	2.07	1.70
CPP modi. TiO_2	0.9	1.0	10.13	24.26		64.38	0.0	1.22
PP modi. TiO_2	1.2	1.5	35.18	14.33		47.73	0.86	1.90
AEP modi. TiO_2	1.1	2.1	21.07	21.23		54.53	1.16	2.02
NPP modi BT	0.8	2.0	19.20	10.37	10.83	53.21	2.40	3.99

Table 2. Thermal and Dielectric Properties Characterization Data for 5 vol. % TiO_2 and BT Polymer Nanocomposites Compared to Pure Polymer

dielectric sample (~60 μm thickness)	T_g (°C)	DBS[a] (V·μm^{-1})	β[a]	dielectric constant[b] at 10 kHz	dielectric loss[b] at 1 kHz	dielectric loss[b] at 10 kHz	leakage current density[c] (pA·cm^{-2})	max. energy density[d] (J·cm^{-3})
pure polymer (Epoxy)	99	288	14	4.0	<0.010	<0.017	1.1	1.4
TiO_2 epoxy	85	247	21	5.8	<0.015	<0.024	11.7	1.6
AEP modi.TiO_2 epoxy	97	307	22	6.4	<0.015	<0.024	6.9	2.7
APP modi.TiO_2 epoxy	95	309	13	5.5	<0.012	<0.021	6.0	2.3
CPP modi.TiO_2 epoxy	97.3	340	19	5.6	<0.013	<0.021	5.6	2.9
NPP modi.TiO_2 epoxy	100	368	16	5.3	<0.012	<0.020	4.4	3.2
PP modi.TiO_2 epoxy	96.5	271	38	5.3	<0.012	<0.018	7.9	1.7
BT epoxy	93	310	30	6.8	<0.012	<0.021	3.1	2.9
NPP modi. BT epoxy	96	383	27	6.3	<0.011	<0.018	2.1	4.1

[a]Obtained as E_o and β, respectively, from Weibull distribution plots of DBS measurements. [b]Measured at room temperature. [c]Measured at 100 V_{DC} for a 31.67 mm^2 circular area and at room temperature. [d]Maximum energy densities were calculated using average relative permittivity measured at 10 kHz and the Weibull distribution intercept (E_o) for DBS.

ships might also be predictive of new, advantageous surface modification structures.

RESULTS AND DISCUSSION

After reacting the metal oxide filler surfaces of either titania or barium titanate (BT) with an organophosphate to form SAM modified nanoparticles, the particles were first assessed for quantity of organic groups. Thermogravimetric analysis (TGA) and X-ray photoelectron spectroscopy (XPS) measurements of surface modified nanopowders are shown in Table 1. The modified nanopowders were extensively washed to remove any physisorbed or unreacted excess reagent prior to analysis and use in composites. Significant organic weight loss was observed above 200 °C for the organophosphate ligand; modifications were due to thermal decomposition and volatilization of organic residues.[25−27]

Organic weight loss data for SAM analysis corresponded to grafting densities of 1.0−2.1 groups/nm^2. Grafting densities were about one-fourth to one-half that of the theoretical assumption of grafting density of ~4.2 organophosphonate groups/nm^2 for highly ordered SAMs.[28] A polycrystalline surface nature of nanosized metal-oxide particles and multidentate bonding observed for the phosphate groups on particle surfaces may be responsible for less ordered monolayer surfaces. Unlike silanes, which are capable of self-polymerization prior to surface bonding and reported to yield nonuniform multilayer film growth on the particle surface,[28] a SAM film growth mechanism is possible for phosphates that minimize the capability for diffuse, multilayer surface deposition.

XPS measurements indicated the introduction of phosphorus groups on the surface modified samples and relatively uniform and consistent surface modification across the organophosphate ligands. The surface modified powders showed mainly bridged phosphate oxygen at ~531.4 eV (P−O−Ti, P═O) and ~532.6 eV (R−O−P, where R is alkyl or phenyl carbon).[29,30] Bonding of coupling agents on the surface of titania or barium titanate via phosphate oxygen appears mostly tridentate, which was assessed by the oxygen peak area ratio between ~531.4 eV to ~532.6 eV, respectively. Thus, both TGA and XPS measurements support a consistent, chemically strong surface bonding by organophosphate ligands onto the surface of nano filler particles by the surface modification reactions.

The polymer glass transition temperature (T_g) is related to the interaction strength and free volume of polymer chains.[31] Polymer nanoparticle composites with unmodified fillers have shown a decreased glass transition temperature,[13,14] which has been observed to be affected by the radius of curvature of the particles increasing the free volume of polymer chains at the interface.[32] For example, the pure epoxy polymer shows a glass transition temperature of about 99 °C. Bare TiO_2 nanoparticle filled composites, with addition of an adsorptive surfactant in the composite to aid dispersion of filler, are observed to increase the free volume of the interfacial polymer chains as shown by a depressed T_g, lowered by 13 to 15 °C versus pure polymer (Table 2). Bare BT particle composites with surfactant/dispersant similarly depressed polymer T_g, 6 to 8 °C less compared to pure polymer.

Particles that increase the free volume of the interfacial polymer chains due to weakly adsorbed interfaces would also be expected to reduce electromechanical strength.[31] DBS of the polymer nanoparticle composites is shown in Table 2. An increased free volume of the chains expressed as lower T_g values, at the interface around filler particles appears to have a

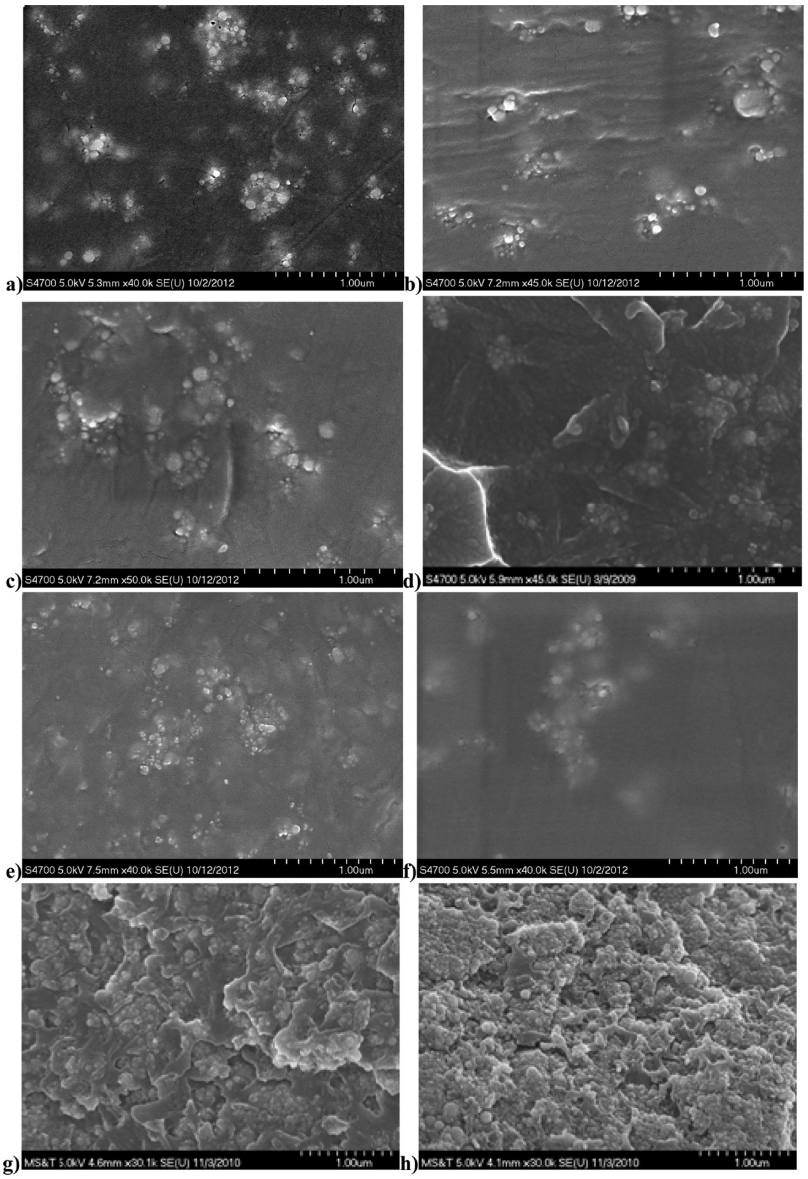

Figure 2. Cross sectional SEM images of nanocomposite dielectric films. (a) NanoTiO_2epoxy (with surfactant, BYK-w-9010), (b) PPmodi.NanoTiO_2epoxy, (c) APPmodi.NanoTiO_2epoxy, (d) AEPmodi.NanoTiO_2epoxy, (e) CPPmodi.NanoTiO_2epoxy, (f) NPPmodi.Nano-TiO_2epoxy, (Note: a to f images are at 5 vol % particle loadings) (g) and (h) are 15 vol % and 30 vol % images of NPPmodi.NanoTiO_2epoxy. Images (a) through (f) are of polished samples while (g) and (h) are freeze fractured samples.

similar effect as increased crystallinity, although the polymer matrix is amorphous. An intercrystalline gallery spacing parallel to the applied field lengthens the mean free path of an accelerated electron and decreases DBS.[33]

Interfacial adsorption has been shown to affect polymer chain density and mobility at the interface.[34−36] Unlike TiO_2 polymer composites, BT polymer composites with adsorbed surfactant molecules showed slightly improved DBS compared to pure polymer that may be due to better dispersibility of BT particles in epoxy matrix compared to bare TiO_2 particles, owing to the relatively lower surface energy and lower inherent surface conductivity of BT nanoparticles compared with nanotitania (please refer to the Nyquist plot provided in Figure 4). Previous research studies[12,37−39] of nanometer sized BT polymer composites for electrical insulation applications have reported a range of DBS results from slight reductions to significant improvements when compared to the respective, unfilled polymer films. The formation of a more stable, complexed organic oxide interface that increases polymer T_g values via an organophosphate ligand analogous to the surface modified TiO_2 and BT composites reported here have correlated to improved DBS.[12,14−16,40]

The polished cross sections imaged by field emission scanning electron microscopy (FESEM) for TiO_2 nanocomposites of 5 vol % particle concentration are shown in Figure 2. Surprisingly, nanocomposites with or without dispersant versus organophosphate SAM ligand modified powder nanocomposites yielded little change in particle dispersion quality.

Table 3 presents the dispersion analysis of the imaged cross sections through particle separation distance measurement. Average with standard deviation of interparticle spacings are provided. Little difference is observed in the quality of dispersion where SAM modified particles have dispersion

Table 3. Dispersion Quality Analysis of Polished Composite Cross Section FESEM Images for 5 vol % TiO_2 Concentration in Epoxy

SAM modification	average separation (nm)	standard deviation
none (dispersant)	954	486
APP	849	558
PP	1166	758
CPP	777	445
NPP	802	673

quality equivalent to that of bare particles with the assistance of an added dispersant. Use of energy dispersive X-ray detection was attempted to improve contrast but could not provide sufficient resolution to improve the FESEM image analysis.

Transmission electron microscopic images of dispersions are quite similar to the FESEM images (Figure 2) at both lower (500X) and higher (15000 to 30000X) magnifications (see Supporting Information for TEM images). All dispersions are observed to be composed of small similarly sized flocculates with an occasional larger flocculate, with micrometer order separation between flocculates and similar presence of the larger flocculates. The particle separation distance averages in Table 3 then appear mostly representative of interflocculate particle separations rather than intraflocculate particle separations. Intraflocculate distances also appear similar in high magnification TEM images.

The largest average interflocculate/interparticle distances were measured for the PP ligand and also a larger standard deviation. Correlation factors of −0.73 and +0.53 were calculated for average interparticle distances versus breakdown strength and leakage current, respectively, which are both weak correlations and reverse trend correlations to those expected for interparticle separation affecting breakdown strength and leakage current. Dispersion quality was not significantly improved by the use of a chemically bound surface group compared to an unbound, surfactant dispersant additive; however, our data does support that properties observed for SAM surface groups on particles do not correlate to changes in particle dispersion quality.

Table 2 shows the dielectric properties of 5 vol % TiO_2-epoxy nanocomposites using different functional groups containing organophosphate coupling agents. An electron withdrawing, electropositive phenyl organophosphate coupling agent, that is, NPP or CPP, when used to modify the surface of TiO_2 produced significantly improved DBS when compared to the pure epoxy polymer, an unmodified TiO_2 composite, or an electron rich phenyl organophosphate modified TiO_2 composite. DBS data in Table 2 resulted from a Weibull statistical failure analysis (eq 2) method.[12,41] In eq 2, $P_F(E_b)$ is equated to median-ranked positioning of sample occurrence within a test population and E_b are measured DBS values.[12,40] The discrete measurements are merged from multiple measurements of multiple samples' results and are expected to thus show population statistical DBS. The scale parameter, α, represents the field intensity corresponding to a 63.2% breakdown probability (P_F).

$$\log[-\ln\{1 - P_F(E_b)\}] = \beta \log E_b - \beta \log \alpha \quad (2)$$

The shape parameter, β, shows the dispersion and consistency of the DBS values (Table 2). The higher the β value, the lower the spread of the data points and more reproducible and consistent are the DBS results.[41] The β values for our composite data sets vary from 13 to 38, which are similar to or greater than that of the pure polymer data set. The β indicate a small relative standard deviation compared to common literature values and of composites compared to polymer alone and reflect consistent measurements of the material DBS.[42] The β values obtained here, in conjunction with other characterizations, are then indicative of consistent and reproducible sample preparation and DBS measurement.

An unmodified, bare TiO_2 filled composite dispersed using adsorptive surfactant showed DBS lower than a pure epoxy polymer, which agreed with previously reported composite results.[14] Surface modification of the filler surfaces as described here improved dielectric properties, that is, dielectric loss, leakage current, and DBS.[14−19]

However, permittivity remained a simple function of filler volume within the composite. Dielectric constants obtained at room temperature using surface modified TiO_2 nanocompo-

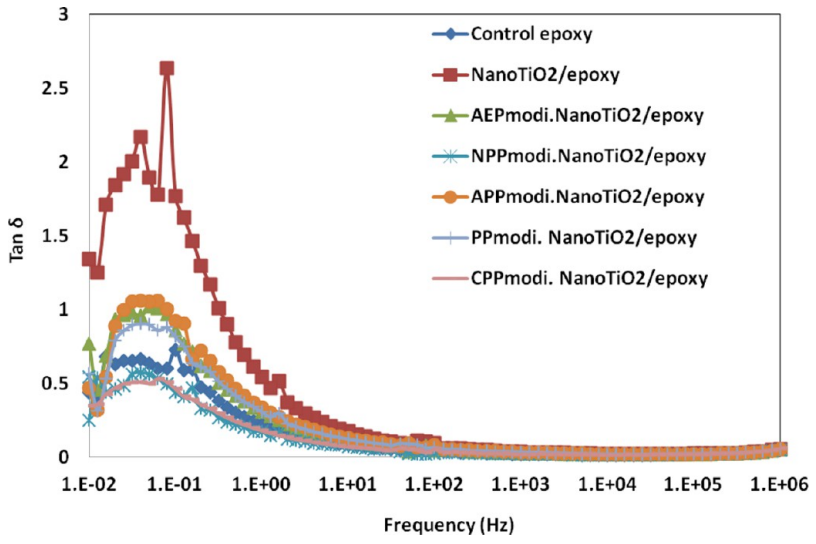

Figure 3. Frequency dependent dielectric loss response of pure polymer and 5 vol % TiO_2 epoxy dielectric composites at lower frequencies that shows MW relaxation loss, measured at 100 °C to increase the signal-to-noise ratio and the transition frequency.

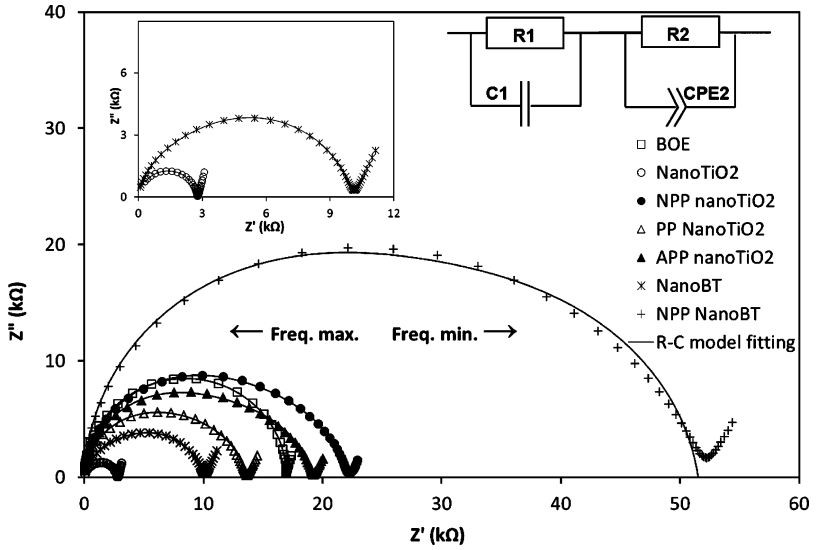

Figure 4. Nyquist plot of impedance spectra for 20 vol % TiO_2 and BT based powders' slurries in a butoxyethanol suspension fluid showing control of surface conductivity for SAM modified powder varies as a function of the SAM structure. Inset are bare nanoparticle dispersion slurry impedance spectra and the equivalent circuit model used to extract solvent and particle resistance. R1 and R2 are solvent and particle resistance values, respectively, C1 and CPE2 are solvent capacitance and constant phase element of the particles, respectively. R-C model fit shows the equivalent circuit behavior.

Table 4. Equivalent Circuit Model Fitting Parameters of Impedance Data and the Permittivity Values Obtained for the Solvent and Particle Circuit Elements of the Samples[a]

sample	R1 (kΩ)	C1 (F)	R2 (kΩ)	CPE2-T (F)	CPE2-P	C2 (F)	$\varepsilon_r{}^b$	$\varepsilon_r{}^c$
BOE	16.9	1.70×10^{-10}	-	-	-	-	9.8	-
Nano TiO_2	2.7	2.87×10^{-10}	-	-	-	-	18.7	-
PP Nano TiO_2	7.1	2.92×10^{-10}	6.4	2.82×10^{-09}	0.88	6.91×10^{-10}	18.9	45
APP Nano TiO_2	10.0	2.70×10^{-10}	9.2	3.86×10^{-09}	0.86	7.51×10^{-10}	17.5	50
NPP NanoTiO_2	11.9	2.72×10^{-10}	10.2	5.50×10^{-09}	0.85	1.04×10^{-09}	17.7	70
NanoBT	10.1	4.50×10^{-10}	-	-	-	-	25.1	-
NPP NanoBT	25.4	5.00×10^{-10}	26.1	5.90×10^{-09}	0.90	2.20×10^{-09}	28.4	135

[a]Positions showing "-" were not resolvable using the equivalent circuit approach. Solvent is assigned as phase 1 and particles as phase 2. R columns provide circuit resistor values and C columns provide phase capacitance. CPE columns show the values of a constant phase element within the particle circuit element of effective capacitance (T) and phase angle (P). [b]Permittivity of liquid (solvent) component of the slurry. [c]Permittivity of particulate component of the slurry.

sites were comparable to those of unmodified TiO_2 particle nanocomposites. The filler surface modification did not significantly alter composite permittivity, even of the high surface area per volume nanocomposites or at higher filler concentration.

Results pertinent to this study were associated with space charge phenomena, significantly reduced leakage currents (Table 2), reduced Maxwell–Wagner (MW, tan δ) dielectric relaxations for composites utilizing surface modified fillers (Figure 3), and greater particle surface impedance measured through impedance spectroscopy (Figure 4 and Table 4). More electropositive phenyl organophosphate SAMs, for example, NPP, modifying the surface of the TiO_2 filler showed significantly lower leakage currents, a corresponding lower dielectric loss across the frequency spectrum, and reduced particle surface conductivity compared to an unmodified, bare TiO_2 particle composite, more electron rich phenyl SAM organophosphate modified TiO_2 particle composites, or even to the pure polymer. Lower leakage current, dielectric loss, and reduced particle surface space charge are each essential for optimal energy storage and peak-load leveling applications.[43] Difference in leakage current densities and dielectric losses between TiO_2 and BT polymer composites has been attributed to space charge differences that occur in different types of composites.[44]

The impedance spectra of the particle slurries were subjected to equivalent circuit modeling to deconvolute the solvent element contributions from particle element contributions.[19,45,46] The equivalent circuit model results are provided in Table 4. Two phenomena that result from SAM modification are shown in the data. First, solvent impedance was improved by the presence of the SAM layer, which appears to offer chemical passivation properties to the particle surface to prevent conductive species from dissolving/desorbing from the particle surface into the solvent. The surface passivation effect would also be of use to prevent contamination of the insulating polymer matrix of the composite and help resist leakage current and breakdown. Second, the SAM provides reduced particle surface conductivity (R2) that is analogous to improvements in leakage current and dielectric breakdown strengths observed as a function of the SAM structure. Bare particles were found sufficiently conductive that they resemble metallic particles where the applied field is effectively excluded from the particle interiors and no distinct particle impedance relaxation is

observed. This effect also would serve to reduce leakage current and improve resistance to dielectric breakdown.

While organophosphate ligand SAM modified filler nanocomposites may also yield improved DBS and low leakage currents because of effective chemical surface passivation of nanoparticles and reduced nanoparticle aggregate formation,[16,19] our study suggests that the surface of TiO_2 particles is best modified with electropositive aromatic organophosphate ligands that, for example, contain an electron withdrawing functional group such as nitro, which showed improved leakage current (<5 pA-cm^{-2} at 100 V), dielectric loss, and DBS compared to electron donating functional group modified TiO_2 composites.

We here present that the electronic nature of the particle's surface, based on the type of functional group of the organophosphate ligand, correlated with improvements observed in the dielectric properties. Electrostatic potential maps of various functional groups containing organophosphate surface modifiers (Figure 5) suggest that the electron

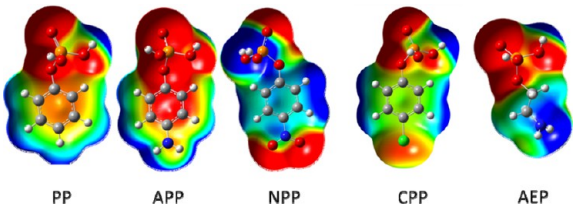

Figure 5. Electrostatic potential maps of surface modifiers obtained from DFT modeling. Red color indicates negative charge, whereas blue color indicates positive charge.

withdrawing group induces the aromatic ring to be more positive (i.e., electron withdrawing) versus other surface ligands. To further examine this correlation, our hypothesis was that the electronic structure effect of the organophosphate group should correlate to leakage current and DBS, which could perhaps be visualized through a Hammett relationship. The Hammett relationship would thus enable correlation of group polarity and/or electron delocalization contribution(s) to predict dielectric properties.

A Hammett equation (eq 3), where m is a proportionality (slope) constant and σ is the substituent property variable, is usually used to study electronic structure-rate reactivity relationships for compounds containing substituted phenyl groups in a reaction process.

$$m\sigma = \log(k/k_0) \quad (3)$$

The effect of the substituent group on the free energy of ionization of the substituted phenyl group giving rise to difference in reaction rates (k).[22−24] We suggest that a rate of reaction ratio expressed by the Hammett relationship may be analogous to an ability for electron or ion absorption or trap depth.

To correlate a surface functional group to Weibull DBS (E) and leakage current ($i_{l\sigma}$) of nanocomposites, we plotted log (E/E_o) and log ($i_{l\sigma}/i_{lo}$) versus Hammett constants, σ, of the phenyl group substituent. Chemical structural factors like resonance, polarity, position of substituent, and so forth contribute to the substituent Hammett constant for which tables of values exist.[22−24] The para substituent position on the phenyl ring is a combined effect of polarity and resonance contributions by the substituent group (σ_p), whereas constants also exist that isolate group polarity (σ_l) and/or group resonance (σ_r) contributions of the substituent that may be responsible for differences in reactivity.[22−24] Plotting the log rate against combined (σ_p) or discrete (σ_l, σ_r) Hammett constants allows changes in reactivity to be correlated to combined or discrete polarity and/or resonance functional group contribution(s), respectively.

The correlation of leakage current and DBS against Hammett substituent constants is summarized in Table 5. From these

Table 5. Correlation of Leakage Current ($i_{l\sigma}$) and Weibull DBS (E_σ) for the Substituted Phenyl Group Phosphate Ligand-Modified-Filler Composite[a] Films against Hammett Substituent Constants for the Phenyl Group Substituents of the Organophosphate Surface Modifier

substituent group	log ($i_{l\sigma}$/ i_{lo})[b]	log (E_σ/E_o)[b]	σ_p[c]	σ_l[d]	σ_r[e]
hydrogen	0.00	0.00	0.00	0.00	0.00
amino	−0.12	0.06	−0.66	0.17	−0.80
chloro	−0.15	0.10	0.23	0.47	−0.25
nitro	−0.25	0.13	0.78	0.67	0.10

[a]Composites are 5 vol % TiO_2-epoxy based nanocomposites. The leakage current and DBS values of the phenyl phosphate modified filler composite films, whose ligand bears the "Hydrogen" substituent on the phenyl ring, are the traditional Hammett reference values (i.e., i_{lo}, E_o) [b]Calculated from the values reported in Table 2. [c]The para position Hammett substituent constants of combined polarity and resonance effects. [d]tThe polarity effect substituent constants. [e]The resonance effect substituent constants.

results, the polarity effect constants of the ligand substituents show linear, Hammett relationships to leakage current and DBS (Figure 6a), whereas linear trends were not observed with either the para substituent (combined polarity and resonance) effect or only resonance effect contribution Hammett substituent constants (Figures 6b and 6c, respectively). A weak para effect Hammett constant correlation appears because of the polarity component that is part of the para constant. Hence, greater electropositive polarity was observed to correlate to minimized leakage current and maximized DBS. Hammett correlation might then prove useful as a tool in the design of new interfaces to reduce surface conductivity of inorganic oxides, for example, to improve composite DBS.

Improved energy storage density (Table 2) was observed for the composite system possessing the more electropositive, electron withdrawing functional group (i.e., nitro group) containing interface as a result of the improved leakage current, dielectric loss, and DBS. DBS is limited in practical terms by current-promoting defects introduced during film manufacture.[47] Hence, conductive paths are relatively easier to form for thicker dielectric films compared to thinner films.[48−50] Our study of DBS as a function of film thickness (Table 6) also demonstrated further improvement in DBS and calculated energy densities for thinner films. Decreasing film thickness also corresponded with an increase in the Weibull β values of the DBS measurements which would correlate to a reduction in current-promoting defects at lower dielectric film thickness. At a dielectric film thickness of ∼15 μm, a calculated energy density of ∼5 J·cm^{-3} was observed through combined improvements in permittivity and DBS for NPP modified nano TiO_2 in epoxy composites at a 5 vol % particle concentration.

Previous study[43] suggests that the volume fraction of the high dielectric constant nanoparticles has to be increased above a

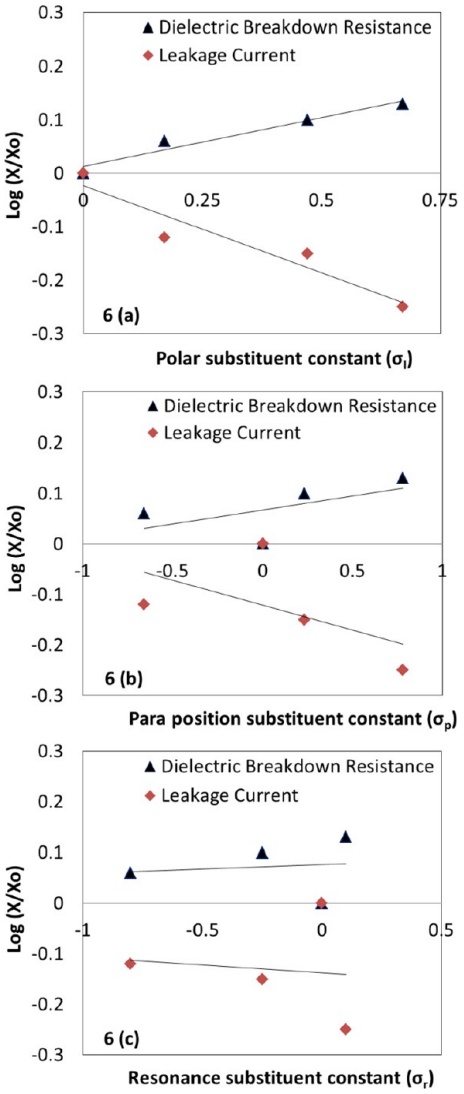

Figure 6. Plots showing Hammett correlation with dielectric breakdown resistance and leakage current. (a) Polar effect of the substituents; (b) para position effect of the substituents; and (c) resonance effect of the substituents.

Table 6. Influence of Dielectric Film Thickness on DBS and Overall Energy Density of 5 vol % NPP modi.TiO_2 Epoxy Nanocomposites

thickness (μm)	DBS (V·μm^{-1})	β values	max. energy density (J·cm^{-3})
60	368.1	16	3.2
45	396.1	27	3.7
15	460.2	29	5.0

certain threshold, typically 30%, to effectively increase the nanocomposite dielectric constant. On the other hand, nanoparticle volume fractions greater than 40 vol % typically decrease the effective dielectric constant of the nanocomposite because of increased porosity and packing defects.[40] An increasing volume fraction of the nanoparticles typically increases leakage current, MW conductive loss, defect conductivity, and a local enhancement of the electric field which decreases the DBS of the nanocomposite.[39,40,46,51,52] Volume concentrations of filler greater than ~50 vol % also reduce the composite adhesion, flexibility, and mechanical durability. At higher filler loadings, one can compromise DBS against the dielectric constant to increase energy storage density.[53]

The dielectric properties for NPP modified nano TiO_2 and BT composites in epoxy at different filler loadings is shown in Table 7. At a loading of 30 vol % TiO_2 filler, modified with NPP, and a composite film thickness of ~15 μm, a maximum energy density of ~8 J·cm^{-3} was calculated. A tan δ loss of ~2.2% was measured for the 30 vol % NPP TiO_2 filler films. An increase in leakage current density with increase in particle concentration is mainly attributed to anisotropic agglomeration[42] and particle associated structure defects[54] induced by a high concentration of metal-oxide particles. Indeed, DBS correlated inversely with these defects assessed by leakage current (i_l).

At the 30 vol % filler loading with more electron withdrawing functional group (nitro) containing interface, NPP modified nanoBT filler, and ~20 μm dielectric film thickness, an energy storage density of ~8.5 J·cm^{-3} was calculated (Table 7). The 30 vol % NPP BT filled composite film had a measured tan δ loss of around 2.5%.

Polarization as a function of electric field of the NPP modified nanoBT−epoxy composites (Figure 7) was also measured. Samples at 5 vol % particle concentration displayed linear dielectric character compared to nonlinear, ferroelectric behavior observed at the higher particle concentration of 30 vol %. The energy storage efficiency, as the ratio of reversible energy of discharge to total energy stored during charging, of the 30 vol % NPP modified nanoBT-epoxy composites was about 74% under an applied field of 52.4 V·μm^{-1} and measured to be about 0.41 J·cm^{-3}. Assuming a linear response, the projected energy storage density at a fairly conservative dielectric field of 250 V·μm^{-1}, 74% of the minimum measured DBS failure (339 kV/μm) observed in the statistical Weibull distribution of DBS, was ~9.5 J·cm^{-3}.

CONCLUSIONS

We demonstrate that SAM surface groups attached to the surface of nanoparticle TiO_2 or nanoparticle BT filler particles influenced dielectric leakage current, tan δ loss, DBS, and

Table 7. Dielectric Properties at Various Volume Fractions of NPP Modified Nano TiO_2 and BT Epoxy Composites

composite (15−20 μm thickness)	DBS (V·μm^{-1})	β values	dielectric constant at 10 kHz	dielectric loss at 10 kHz	dielectric loss at 1 kHz	leakage current density (pA·cm^{-2})	max. energy density (J·cm^{-3})
5 vol % TiO_2 epoxy	460	29	5.3	<0.020	<0.012	5.4	5.0
15 vol % TiO_2 epoxy	425	27	7.1	<0.021	<0.018	28.5	5.7
30 vol % TiO_2 epoxy	355	30	14.4	<0.022	<0.021	539.5	8.0
5 vol % BT epoxy[a]	431	33	6.1	<0.020	<0.013		5.0
30 vol % BT epoxy	300	30	21.3	<0.025	<0.025	301.5	8.5

[a]Film thickness ~30 μm.

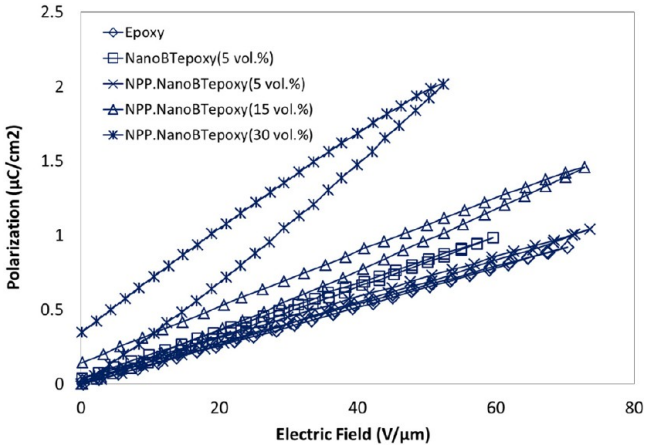

Figure 7. Polarization versus electric field of NPP modified nanoBT-epoxy composites as a function of filler volume concentration compared to pure epoxy polymer.

energy storage density of the polymer−particle nanocomposite dielectric films. Our characterizations support the hypothesis that the electronic structure of the filler ligands can indeed control the dielectric properties of the composite. A linear Hammett relationship against the surface group polarity effect suggests that other electropositive ligands may be useful for particle surface modification to minimize leakage current and dielectric loss and provide for higher DBS for improved energy storage density in dielectric composites. However, Hammett constants involving both polarity and resonance effects or only resonance-specific Hammett effects did not correlate to leakage current or DBS performance. The surface modification methodology is straightforward and appears easily adaptable to most metal oxide filler materials, with suitable choice of aromatic electron withdrawing functional group, to polymer-ceramic dielectric composite systems.

EXPERIMENTAL METHODS

Chemicals. The chemicals and reagents were obtained from the following sources and were used without further purification. Titanium dioxide, anatase in structure, of average particle size 32 nm and surface area of 45 $m^2 \cdot g^{-1}$ was obtained from Alfa Aesar. Barium titanate of average particle size 30−50 nm and 14 $m^2 \cdot g^{-1}$ average surface area was obtained from Sigma Aldrich.

The surfactant BYK-w-9010 is a proprietary copolymer mixture of polyester containing phosphoric acid functional groups, which is recommended for inorganic pigment dispersion use in epoxies and unsaturated polyester resin systems. It is a solvent-free, commercial product of Byk-Chimie with a reported acid value of 129 mg KOH/g. The chemical 2-aminoethyl phosphate (AEP) was obtained from Sigma Aldrich. Phenyl phosphate (PP) was obtained from Acros Organics. The solid 4-nitrophenyl phosphate (NPP) was obtained from Chem Impex International. Aminophenyl phosphate (APP) was synthesized from NPP as mentioned before.[55] Chlorophenyl phosphate (CPP) was obtained by hydrolysis of 4-chlorophenyl phosphorodichloridate that was obtained from Sigma Aldrich. Water was distilled−deionized and of 1 $M\Omega \cdot cm^{-1}$ resistance. Epoxy resin (trade name Epon 828) was obtained from Hexion. The polyamide resinous curing agent used was a moderately low molecular weight, liquid blend of the commercial products Ancamide 2353 and Ancamine 2205 at a 3:1 ratio and activated with 5 vol % Ancamine K-54. The Ancamide 2353, Ancamines 2205, and K-54 were obtained from Air Products.

Surface Modification of Titania and Barium Titanate. In a typical surface modification reaction, TiO_2 nanoparticles were dispersed in water (distilled and deionized) and degassed by sonication while under aspirator-reduced pressure for 15 min. Organophosphate ligand, approximately 6−10 wt % of particle mass was mixed with a nano titania dispersion and stirred at reflux conditions for 24 h. The surface modified nanoTiO_2 particles were then recovered by filtration followed by redispersion in fresh water and filtration, repeated four times to remove any excess and/or physisorbed ligand. The treated TiO_2 nanoparticles were dried thoroughly in a vacuum oven before preparing composites in epoxy. The surface of nano $BaTiO_3$ particles were modified as described before[15] but using NPP.

Particle Characterization. For obtaining electrostatic potential maps of the surface modifiers, structures were created and optimized using AVDZ (augmented double-ζ) as the basis before optimizing the geometry of the molecules using the DFT (density functional theory) and B3LYP method. Gaussian 09 software and Gaussview 5.0.9 interface were employed for generation and visualization of models.

Surface treated and untreated nano particles were characterized by XPS and TGA as described before.[14] Particle permittivity and surface conductivity of the bulk insulating particles were assessed before and after surface modification with the SAMs by a powder slurry in Maxwell liquid methodology.[56]

The impedance powder-solvent slurry samples were prepared by dispersing 15 g of oven-dried powder (175 °C, 6 h) using first mechanical convection followed by ultrasound from a Vibra-Cell system (Sonic & Materials Inc., Danbury, CT; VCX 1500 amplifier, CV 294 converter, tapered 6 mm microtip) for a maximum of 2 min at a 300 W output power before impedance spectroscopy measurement. The gravimetric settling of nanoparticle and microparticle slurries was observed though no consequence on the impedance of the slurry was observed within time of measurement. An electrochemical cell with stainless electrodes (surface area: 4 cm^2; separation distance between the electrodes: 0.2 mm) was assembled as a sample cell for conducting the slurry electrical characterization. An automated Solartron system, Solartron 1260 impedance analyzer connected with a Solartron 1296 dielectric interface (Solartron analytical, Hampshire, England) in the frequency range of 100 mHz to 1 MHz and voltage amplitude of 100 mV was used to collect the impedance data.

Composite Preparation. Composite films were made by first dispersing particles into polyamide resin via a ball-milling process overnight (~16−18 h). A separate dispersant, the BYK-w-9010, was added only to a bare particle dispersion of TiO_2/BT in polyamide as an experimental control to compare a dispersed particle composite against a self-dispersing (surface modified) particle, where the particle uses the bound surface groups to aid its dispersion. The ball-milled dispersion was sieved to remove the ball media into a clean, preweighed jar. Epoxy resin in amount stoichiometric to the amount of polyamide was added to the dispersion, and the uncured, liquid composite stirred for 5 min before degassing. Films of the uncured, liquid composite were applied to freshly exposed, polished copper (Electronic grade 110 alloy, 0.8125 mm thick, #8 finish, obtained from McMaster Carr). Composites were allowed to initially cure overnight at room temperature in a dust-free vented cabinet, followed by completing the polymer matrix cross-linking process by baking in a forced-air conventional oven at 80 °C for 24 h followed by 100 °C for 6 days. A 6 day cure was found necessary to remove all volatiles from the film and maximize DBS.

Composite Characterization. Completely cured composite films and pure epoxy polymer were characterized by differential scanning calorimetry (DSC) for T_g, electrical impedance, and DBS as described before.[14] To observe Maxwell−Wagner particle relaxation (tan δ) losses at lower frequencies, electric impedance measurements were performed at 100 °C to enhance the composite conductivity signal and reduce low frequency signal noise. Film thicknesses were measured with a Mitutoyo 0293-340 micrometer and subtracting the thickness of the copper substrate.

A Hitachi S-4700 FESEM was used for obtaining SEM images of film cross sections of dielectric composite films for examining the quality of dispersion. Samples were wet-abrasive wheel polished using successively fine grit and finally polished with a cloth wheel and 1 μm silica dispersion. FESEM images were subjected to particle size analysis

utilizing ImageJ software[57] by manual input of particle positions as visible in the SEM (results shown in Table 3). Correlation factors between average particle separation and DBS and leakage current values (from Tables 2 and 3) using the equation: Correl(X:Y) = $\Sigma(X - \bar{X})(Y - \bar{Y})/((X - \bar{X})^2(Y - \bar{Y})^2)^{1/2}$, where X and Y are values from each data array and the bar values are the average values of each array being correlated.

Additional visualization of dispersion quality was provided by TEM microtoming and imaging (JEOL 1400 with lanthanum hexaboride filament at 80 kV accelerating voltage) of dispersions at low (500×, Supporting Information) and high (30000×) magnifications. TEM images further support the dispersion structure analysis of FESEM images as provided in the Results and Discussion. Freeze fractured samples were immersed in liquid nitrogen, and broken and visualized in the FESEM.

Dielectric breakdown strength measurements were made by applying DC voltage across the films using a Spellman SL 30 high voltage generator (Spellman High Voltage Electronics Corporation, New York, U.S.A.), with a fixed ramp rate of 200 V/second until the point of catastrophic device failure was observed. A pin electrode was applied by spring tension to the surface of the composite, which served as the electrical ground. The Spellman electrode was connected beneath the copper substrate and the sample immersed in Fluorinert FC-40 (Acros Scientific) to displace air. Five to ten DBS measurements were made to each of at least three sample film experiments for each composition whose data were combined and analyzed by a Weibull distribution plot.

Leakage current measurements were performed using a Keithley 6517 Electrometer (Keithley Instruments, Cleveland, U.S.A.) at room temperature and 100 V_{DC} bias. Polarization as a function of electric field was measured with a ferroelectric tester (RT6000, Radiant Technology, NM, U.S.A.) for nonlinear/ferroelectric BT based dielectric composites.

■ ASSOCIATED CONTENT

Supporting Information

High contrast images of each sample were acquired by TEM at two magnifications, low (500×) and high (30000×), as described in the Composites Characterization Experimental Methods section, and are provided as Supporting Information. The images support the discussion and conclusions about the quality of particle dispersion in the dielectric composites that were also characterized by SEM analyses of polished cross sections. This material is available free of charge via the Internet at http://pubs.acs.org.

■ AUTHOR INFORMATION

Corresponding Author

*E-mail: tschuman@mst.edu.

Notes

The authors declare no competing financial interest.

■ ACKNOWLEDGMENTS

This material is based upon work supported by the National Science Foundation, as part of the Pennsylvania State University-Missouri S&T I/UCRC for Dielectric Studies under Grant 0628817, Sub-Award No. 2164-UM-NSF-0812 and by U.S. Office of Naval Research award No. N00014-11-1-0494. The authors acknowledge the assistance of Phalgun Lolur and Richard Dawes for electrostatic potential map simulations, Vladimir Petrovsky for assistance with leakage current measurements, and analytical support provided by the Materials Research Center facilities at the Missouri University of Science and Technology. Microtome and TEM images were provided by Juliana Vinson at the Electron Microscopy Core Facility at University of Missouri, Columbia, Missouri.

■ REFERENCES

(1) Cheng, L.; Zheng, L.; Li, G.; Zeng, J.; Yin, Q. *Phys. B* **2008**, *403*, 2584−2589.
(2) Chu, B.; Zhou, X.; Ren, K.; Neese, B.; Lin, M.; Wang, Q.; Bauer, F.; Zhang, Q. M. A. *Science* **2006**, *313*, 334−336.
(3) Polizos, G.; Tomer, V.; Manias, E.; Randall, C. A. *J. Appl. Phys.* **2010**, *108*, 074117.
(4) Tuncer, E.; Sauers, I.; James, D. R.; Ellis, A. R.; Paranthaman, M. P.; Goyal, A.; More, K. L. *Nanotechnology* **2007**, *18*, 325704.
(5) Xiaojun, Y.; Zhimin, Y.; Changhui, M.; Jun, D. *Rare Met.* **2006**, *25*, 250−254.
(6) Li, J. Y.; Zhang, L.; Ducharme, S. *Appl. Phys. Lett.* **2007**, *90*, 132901/1−132901/3.
(7) Li, J.; Seok, S.; Chu, B.; Dogan, F.; Zhang, Q.; Wang, Q. *Adv. Mater.* **2009**, *21*, 217−221.
(8) Smith, R. C.; Liang, C.; Landry, M.; Nelson, J. K.; Schadler, L. S. *IEEE Trans. Dielectr. Electr. Insul.* **2008**, *15*, 187−196.
(9) Tanaka, T.; Montanari, G. C.; Mulhaupt, R. *IEEE Trans. Dielectr. Electr. Insul.* **2004**, *11*, 763−784.
(10) Lewis, T. J. *J. Phys. D: Appl. Phys.* **2005**, *38*, 202−212.
(11) Roy, M.; Nelson, J. K.; MacCrone, R. K.; Schadler, L. S.; Reed, C. W.; Keefe, R.; Zenger, W. *IEEE Trans. Dielectr. Electr. Insul.* **2005**, *12*, 629−643.
(12) Tuncer, E.; Sauers, I.; James, D. R.; Ellis, A. R.; Paranthaman, M. P.; Aytug, T.; Sathyamurthy, S.; More, K. L.; Li, J.; Goyal, A. *Nanotechnology* **2007**, *18*, 25703.
(13) Yuan, J.-K.; Yao, S.-H.; Dang, Z.-M.; Sylvestre, A.; Genestoux, M.; Bai, J. *J. Phys. Chem. C* **2011**, *115*, 5515−5521.
(14) Schuman, T. P.; Siddabattuni, S.; Cox, O.; Dogan, F. *Compos. Interfaces* **2010**, *17*, 719−731.
(15) Siddabattuni, S.; Schuman, T. P.; Dogan, F. *Mater. Sci. Eng. B* **2011**, *176*, 1422−1429.
(16) Kim, P.; Jones, S. C.; Hotchkiss, P. J.; Haddock, J. N.; Kippelen, B.; Marder, S. R.; Perry, J. W. *Adv. Mater.* **2007**, *19*, 1001−1005.
(17) Ma, D.; Hugener, T. A.; Siegel, R. W.; Christenson, A.; Martensson, E.; Onneby, C.; Schadler, L. S. *Nanotechnology* **2005**, *16*, 724−731.
(18) Ma, D.; Siegel, R. W.; Hong, J. I.; Schadler, L. S. *J. Mater. Res.* **2004**, *19*, 857−863.
(19) Siddabattuni, S.; Schuman, T. P., Petrovsky, V.; Dogan, F. *J. Am. Ceram. Soc.* accepted in Jan. **2013**. (DOI: 10.1111/jace.12203).
(20) Barber, P.; Balasubramanian, S.; Anguchamy, Y.; Gong, S.; Wibowo, A.; Gao, H.; Ploehn, H. J.; Loye, H.-C. Z. *Materials* **2009**, *2*, 1697−1733.
(21) McMurry, J. In *Organic Chemistry*, 5th ed.; Brooks/Cole: Belmont, CA, 2000; Chapter 16.
(22) Carey, F. A.; Sundberg, R. J. In *Advanced Organic Chemistry−Part A*, 5th ed.; Springer: New York, 2007; Chapter 3.
(23) Charton, M. *Prog. Phys. Org. Chem.* **1981**, *13*, 119−251.
(24) Hansch, C.; Leo, A.; Taft, R. W. *Chem. Rev.* **1991**, *91*, 165−195.
(25) Porkodi, K.; Arokiamary, S. D. *Mater. Charact.* **2007**, *58*, 495−503.
(26) Reid, D. L.; Russo, A. E.; Carro, R. V.; Stephens, M. A.; LePage, A. R.; Spalding, T. C.; Petersen, E. L.; Seal, S. *Nano Lett.* **2007**, *7*, 2157−2161.
(27) Geng, H.; Peng, R.; Han, S.; Gu, X.; Wang, M. *J. Electron. Mater.* **2010**, *39*, 2346−2351.
(28) Helmy, R.; Fadeev, A. Y. *Langmuir* **2002**, *18*, 8924−8928.
(29) Hofer, R.; Textor, M.; Spencer, N. D. *Langmuir* **2001**, *17*, 4014−4020.
(30) Textor, M.; Ruiz, L.; Hofer, R.; Rossi, A.; Feldman, K.; Hähner, G.; Spencer, N. D. *Langmuir* **2000**, *16*, 3257−3271.
(31) Grest, G. S.; Cohen, M. H. *Adv. Chem. Phys.* **1981**, *48*, 455−525.
(32) Blum, F. D.; Sinha, B. R.; Schwab, F. C. *Macromolecules* **1990**, *23*, 3592−3598.
(33) Tanaka, Y.; Ohnuma, N.; Katsunami, K.; Ohki, Y. *IEEE Trans. Electr. Insul.* **1991**, *26*, 258−265.
(34) Blum, F. D.; Lin, W.-Y.; Porter, C. E. *Colloid Polym. Sci.* **2003**, *281*, 197−202.

(35) Zhang, B.; Blum, F. D. *Macromolecules* **2003**, *36*, 8522−8527.
(36) Akabori, K.; Tanaka, K.; Nagamura, T.; Takahara, A.; Kajiyama, T. *J. Cent. South Univ. Technol.* **2007**, *14*, 346−349.
(37) Tuncer, E.; Sauers, I.; James, D. R.; Ellis, A. R.; Duckworth, R. C. *IEEE Trans. Dielectr. Electr. Insul.* **2008**, *15*, 236−242.
(38) Nelson, J. K.; Hu, Y. *J. Phys. D: Appl. Phys.* **2005**, *38*, 213−222.
(39) Gilbert, L. J.; Schuman, T. P.; Dogan, F. Dielectric Powder/Polymer Composites for High Energy Density Capacitors. In *Proceedings of the 107th Annual Meeting of the American Ceramic Society*, Baltimore, MD, 2005; Dogan, F., Kumta, P. M., Eds.; Wiley: Baltimore, MD, 2005; Advances in Electronic and Electrochemical Ceramics.
(40) Kim, P.; Doss, N. M.; Tillotson, J. P.; Hotchkiss, P. J.; Pan, M. J.; Marder, S. R.; Li, J.; Calame, J. P.; Perry, J. W. *ACS Nano* **2009**, *3*, 2581−2592.
(41) Hoyos, M.; Garcia, N.; Navarro, R.; Dardano, A.; Ratto, A.; Guastavino, F.; Tiemblo, P. *J. Polym. Sci., Part B: Polym. Phys.* **2008**, *46*, 1301−1311.
(42) Takala, M.; Ranta, H.; Nevalainen, P.; Pakonen, P.; Pelto, J.; Karttunen, M.; Virtanen, S.; Koivu, V.; Pettersson, M.; Sonerud, B.; Kannus, K. *IEEE Trans. Dielectr. Electr. Insul.* **2010**, *17*, 1259−1267.
(43) Calame, J. P. *J. Appl. Phys.* **2006**, *99*, 084101.
(44) (a) Boggs, S. A. *IEEE Electr. Insul. Mag.* **2004**, *20*, 22−27. (b) Percharroman, C.; Moya, J. S. *Adv. Mater.* **2000**, *12*, 294−297. (c) Pham Thi, M.; Velasco, G.; Colomban, P. *J. Mater. Sci. Lett.* **1986**, *5*, 415−417.
(45) Petrovsky, V.; Dogan, F. *J. Am. Ceram. Soc.* **2009**, *92*, 1054−1058.
(46) Petrovsky, V.; Petrovsky, T.; Kamlapurkar, S.; Dogan, F. *J. Am. Ceram. Soc.* **2008**, *91*, 1814−1816.
(47) Ducharme, S. *ACS Nano* **2009**, *3*, 2447−2450.
(48) Lin, H. C.; Ye, P. D.; Wilk, G. D. *Appl. Phys. Lett.* **2005**, *87*, 182904.
(49) Zhou, H.; Shi, F. G.; Zhao, B. *Microelectron. J.* **2003**, *34*, 259−264.
(50) Kim, H. K.; Shi, F. G. *IEEE Trans. Dielectr. Electr. Insul.* **2001**, *8*, 248−252.
(51) Huang, C.; Zhang, Q. *Adv. Funct. Mater.* **2004**, *14*, 501−506.
(52) Shen, Y.; Lin, Y.; Nan, C. W. *Adv. Funct. Mater.* **2007**, *17*, 2405−2410.
(53) Blonkowski, S. *J. Appl. Phys.* **2010**, *107*, 084109.
(54) Chen, F.-C.; Chuang, C.-S.; Lin, Y.-S.; Kung, L.-J.; Chen, T.-H.; Shieh, H-P. D. *Org. Electron.* **2006**, *7*, 435−439.
(55) Frew, J. E.; Foulds, N. C.; Wilshere, J. M.; Forrow, N. J.; Green, M. J. *J. Electroanal. Chem. Interfacial Electrochem.* **1989**, *266*, 309−316.
(56) Petrovsky, V.; Manohar, A.; Dogan, F. *J. Appl. Phys.* **2006**, *100* (1), 014102−1−4.
(57) Schneider, C. A.; Rasband, W. S.; Eliceiri, K. W. *Nat. Methods* **2012**, *9*, 671−675.